Send Orders of Reprints at reprints@benthamscience.net

368 *Current Molecular Medicine* **2013**, *13*, **368-376**

Multimodal Optical, X-Ray CT, and SPECT Imaging of a Mouse Model of Breast Cancer Lung Metastasis

C.A. Davison[1], S.E. Chapman[4], T.A. Sasser[2,3], C. Wathen[1], J. Diener[4], Z.T. Schafer[1] and W.M. Leevy[*,2,4]

[1]*Department of Biological Sciences, 100 Galvin Life Sciences Center, University of Notre Dame, Notre Dame, IN 46556, USA*

[2]*Department of Chemistry and Biochemistry, 236 Nieuwland Science Hall, University of Notre Dame, Notre Dame, IN 46556, USA*

[3]*Carestream Molecular Imaging, 4 Research Drive, Woodbridge, CT 06525, USA*

[4]*Notre Dame Integrated Imaging Facility, Notre Dame, IN 46556, USA*

Abstract: Tumor heterogeneity is recognized as a major issue within clinical oncology, and the concept of personalized molecular medicine is emerging as a means to mitigate this problem. Given the vast number of cancer types and subtypes, robust pre-clinical models of cancer must be studied to interrogate the molecular mechanisms involved in each scenario. In particular, mouse models of tumor metastasis are of critical importance for pre-clinical cancer research at the cancer cell molecular level. In many of these experimental systems, tumor cells are injected intravenously, and the distribution and proliferation of these cells are subsequently analyzed *via ex vivo* methods. These techniques require large numbers of animals coupled with time-consuming histological preparation and analysis. Herein, we demonstrate the use of two facile and non-invasive imaging techniques to enhance the study of a pre-clinical model of breast cancer metastasis in the lung. Breast cancer cells were labeled with a near-infrared fluorophore that enables their visualization. Upon injection into a living mouse, the distribution of the cells in the body was detected and measured using whole animal fluorescence imaging. X-ray computed tomography (CT) was subsequently used to provide a quantitative measure of longitudinal tumor cell accumulation in the lungs over six weeks. A nuclear probe for lung perfusion, ^{99m}Tc-MAA, was also imaged and tested during the time course using single photon emission computed tomography (SPECT). Our results demonstrate that optical fluorescence methods are useful to visualize cancer cell distribution patterns that occur immediately after injection. Longitudinal imaging with X-ray CT provides a convenient and quantitative avenue to measure tumor growth within the lung space over several weeks. Results with nuclear imaging did not show a correlation between lung perfusion (SPECT) and segmented lung volume (CT). Nevertheless, the combination of animal models and noninvasive optical and CT imaging methods provides better research tools to study cancer cell differences at the molecular level. Ultimately, the knowledge gleaned from these improved studies will aid researchers in uncovering the mechanisms mediating breast cancer metastasis, and eventually improve the treatments of patients in the clinic.

Keywords: Breast cancer, computed tomography (CT), experimental metastasis, fluorescence, optical imaging.

1. INTRODUCTION

Tumor heterogeneity is recognized as a major issue within clinical oncology, and the concept of personalized molecular medicine is emerging as a means to mitigate this problem. In particular, metastatic tumors display an almost infinite heterogeneity that makes treatment extremely difficult. Indeed, metastatic tumors are responsible for approximately 90% of cancer deaths [1]. Metastasis progresses first from a primary site of tumor growth through the initiation of angiogenesis and subsequent invasion of intravascular spaces [2]. Once transported *via* the circulatory system, cells are collected in the capillary beds of remote tissues. Accumulation within capillary beds is mediated by cellular adhesion mechanisms orchestrated by the cancer cells. This is followed by proteolysis and motility of cells to extravascular spaces where secondary metastases develop. Efforts to elucidate the molecular and cellular processes involved in cancer metastasis are ongoing. Multiple molecular mechanisms have been identified as mediators in the establishment of a secondary metastatic site. Several proteins involved in cell adhesion, proteolysis, and motility have been implicated. *In vivo* experimental metastasis protocols have been employed, in conjunction with relevant host and/or tumor cell studies, to delineate the molecular mechanisms associated with

*Address correspondence to this author at the Notre Dame Integrated Imaging Facility, Notre Dame, IN 46556, USA;
Tel: 574-631-1683; Fax: 574-631-6652;
E-mail: wleevy@nd.edu

1875-5666/13 $58.00+.00

the establishment of secondary metastatic sites of breast cancer [3-5].

The traditional experimental metastasis protocol is performed by first administering tumor cells intravenously (IV) *via* the tail vein in mice or rats [6]. Following injection, most cells will localize within the lungs, likely because this is the first capillary bed encountered by systemic circulating cells. Animals are typically sacrificed at 1 to 3 weeks post injection, and the lungs subsequently examined for tumor infiltration and growth using histological methods in conjunction with microscopy. This approach has been employed in numerous studies to yield valuable insights into the underlying molecular mechanisms of metastasis, however the strategy does have limitations. First, it assumes that a consistent dose of tumor cells will be administered to experimental animals. Successful execution of the tail vein injection is a specialized skill, and it has been shown that even the most experienced and capable personnel fail to administer tail vein doses with 100% reliability [7]. The success rate for the novice can be far lower. Furthermore, there is currently no definitive positive indicator that an injection has been properly administered. As a result, experimental animals receiving inconsistent doses can skew experimental findings. Secondly, the current protocol only allows for terminal analysis and does not allow for a longitudinal assessment of disease progression. In many instances, researchers may be interested in molecular mechanisms underlying specific phases of disease progression. Coincident analysis of molecular mechanisms with, and interventions at, specific phases of disease progression is not readily achievable employing these current methods.

With advances in small animal imaging technologies, labels, and techniques, *in vivo* cell tracking and disease monitoring is now feasible. Positron emission tomography (PET), single photon emission tomography (SPECT), computed tomography (CT), magnetic resonance imaging (MRI), and optical imaging with luminescence or fluorescence have all been employed in studies of *in vivo* cell migration [8]. In particular, optical imaging has emerged as a relatively high through-put and cost effective modality for cell tracking. Both endogenous and exogenous optical reporters have been employed for these purposes [9, 10]. Endogenous reporter systems, consisting of cells engineered for expression of a genetic reporter, generally offer higher signal to noise ratios and improved sensitivities compared to exogenous reporters. Genetic reporters are ideal when long term cell tacking is desired because the optical signal is not diluted during cell division; however, production of recombinant cell lines may be time consuming and achieving stable expression of these markers can be challenging [11]. For exogenous labeling, lipophilic near-infrared (NIR) carbocyanine dyes, like 1,1′-Dioctadecyl-3,3,3′,3′-Tetramethylindotricarbocyanine Iodide (DiR), have been adopted for facile pre-labeling of cells for subsequent *in vivo* tracking [12-15]. DiR is an attractive reagent for cell labeling and *in vivo* imaging for several reasons it rapidly and stably inserts into the membranes of most, if not all, cell types in culture. In at least one study, it was shown that DiR did not corrupt the normal behavior of cells [13]. Additionally, the peak fluorescent excitation and emission spectrum of the DiR fall within a range that is compatible with the absorption and scatter properties of tissue required for efficient *in vivo* fluorescent optical imaging. Methods utilizing DiR have been employed mostly for the detection of stem or immune cells in living mice for periods of days to multiple weeks. Reports utilizing DiR for tumor cell tracking are limited [16].

CT imaging has been employed to study disease progression in animal models of emphysema, asthma, pulmonary fibrosis, and pulmonary tumors [17-20]. Small animal CT imaging, compared to other imaging modalities, offers several advantaged for *in vivo* pulmonary tumor imaging. CT scan times are relatively short compared to MRI, PET, and SPECT, and generally provide adequate sensitivity for pulmonary tumor imaging. Additionally, cell labeling and/or contrast agents are not required for CT pulmonary tumor imaging. Several studies of CT tumor imaging in small animals have been reported over the last decade [21-31]. CT imaging of pulmonary tumors has been evaluated in conditional K-ras models, chemically induced urethane models, and models of metastasis. The minimum detectable tumor size varied among reports, but some stated that tumors of 1 mm or less could be resolved. Possible explanations for the disparity in detection levels include differences in detector technologies that provide improved contrast and resolution, as well as varied protocols used for more thorough analysis of entire lung regions. Reports indicate that CT imaging results correlate well with histological data. Some previously reported CT tumor imaging methods have included protocols to segment and quantify lung tumor volumes. These methods generally include manual or semi-automated measures to identify tumor margins for volumetric analysis. Defining accurate tumor margins can be complicated when tumors abut tissues with similar densities. This can occur when tumors occur at the perimeter of the lungs, lie in close proximity to vasculature, or exist in a plane that is adjacent to cardiac tissues.

In these studies, we explored the possibility of utilizing the perfusion agent ^{99m}Tc-MAA and single photon computed tomography (SPECT) to detect changes in vasculature with lung metastasis. ^{99m}Tc-MAA is generally used to assess vasculature function [32, 33]. MDA-MB-231 cells can promote angiogenesis in mouse xenograft experiments [34, 35]. Changes in vasculature may be caused by MDA-MB-231 cell metastasis through induction of angiogenic pathways and/or destruction of natural host vasculature with obstructive tumor growth. ^{99m}Tc-MAA and SPECT imaging has been used to guide clinical radioembolization of hepatic tumors in human patients [36]. It has also been used to evaluate bronchial angiogenesis in a rat model [32]. Therefore, we hypothesized that an increase in lung tumor burden would correlate with a decrease in lung perfusion by

this probe in mice intravenously injected with MDA-MB-231 cells. To our knowledge, ^{99m}Tc-MAA has not been assessed as an agent to monitor changes in lung vasculature function in a small animal tumor model.

Here we describe a modified experimental metastasis protocol, using the breast cancer cell line MDA-MB-231 in conjunction with multimodal optical and CT imaging. This strategy addresses some of the aforementioned limitations of the traditional experimental metastasis protocol. Optical imaging is employed following tail vein injection of DiR labeled cells to confirm a successful injection and directly show that cells have localized to the lungs. Disease progression is subsequently monitored in a longitudinal manner using CT imaging to quantify normal lung density volume. Normal lung density volume analysis is rapid and objective because the analysis includes simple segmentation of the approximate air volume within the lungs of experimental animals. While this method does not return an absolute tumor volume measurement, it is rapid and avoids complications associated with ambiguous tumor margins. In addition, SPECT lung perfusion imaging was performed to evaluate the potential of ^{99m}Tc-MAA to detect changes in lung vasculature during the establishment of a secondary tumor site.

2. MATERIALS AND METHODS

2.1. Cell Culture

MDA-MB-231 cells (ATCC) are derived from the pleural effusion of a breast cancer patient suffering from metastasis years after removal of the primary tumor [37]. MDA-MB-231 cells were cultured in Dulbecco's Modified Eagle Medium (DMEM) (GIBCO) plus 10% FBS (GIBCO), penicillin/streptomycin (Hyclone), and plasmocin (Invitrogen).

2.2. Cell Staining

1,1′-Dioctadecyl-3,3,3′,3′-Tetramethylindotricarbocyanine Iodide (′DiR′; DiIC18(7)) (Invitrogen) was diluted in DMSO to 10 mg/ml. DiR was diluted 1:200 in PBS and added to adherent MDA-MB-231 cells and incubated for 10 minutes at 37℃ according to the manufacturer's protocol. DiR labeled MDA-MB-231 cells were diluted in a 96-well black-walled clear bottom plate in triplicate from 1 X 10^3 to 5 X 10^5 in a two-fold serial dilution. The plate was imaged for DiR fluorescence as described below.

2.3. Mice

Female athymic mice (Foxn1-nu), 5-6 weeks old, were obtained from Harlan Laboratories (Indianapolis, IN). The animals were housed under specific pathogen-free conditions. Three *in vivo* experiments were performed with mice:

1. For an initial study of DiR cell tracking sensitivity during whole animal fluorescence, we injected either 2 x 10^5 (n = 3 mice) or 2 x 10^6 (n = 3 mice) DiR stained MDA-MB-231 cells into the lateral tail vein of nude mice. Imaging was performed for 48 hours as described below.
2. As a control for the cell tracking study, 100 µL of a 5 µg/mL solution (1/10 of cell labeling concentration in buffer) of DiR was injected IV into three mice, which were imaged over 48 hours as described below.
3. For the six week experimental lung metastasis study, 2 x 10^6 DiR stained MDA-MB-231 cells were injected into the lateral tail vein of nude mice (n = 12). A separate cohort of mice (n = 6) was injected with saline to serve as a control. Mice were imaged *via* whole animal fluorescence after 3 h using the methods below. Animals were imaged using SPECT-CT every two weeks as described below. After 6 weeks, the mice were sacrificed and lungs were removed. Lungs were stained in Bouin's solution for 24 hours and stored in 70% ethanol before analysis. Procedures were evaluated and approved by The University of Notre Dame Institutional Animal Care and Use Committee (Protocol 12-115).

2.4. DiR Fluorescence Imaging and Analysis

Fluorescent images (16-bit tiff format) were acquired using the In-Vivo Multispectral FX PRO (Carestream, Woodbridge, CT). DiR fluorescence excitation and emission maxima for membrane-bound dye are 750 nm and 780 nm respectively. Both *in vivo* (under 3% Isofluorane anesthesia) and *in vitro* specimens were irradiated with filtered light of wavelength 750 ± 10 nm, and an image of emission intensity at 830 ± 17.5 nm was collected by a CCD camera during a 30 second acquisition period (bin = 2 x 2, f-stop = 2.51, field of view = 120 mm). ImageJ v1.44 (Research Services Branch, National Institute of Mental Health, Bethesda, MD, USA (available at http://rsbweb.nih.gov/ij/download.html)) was used to perform integrated intensity analysis of regions of interest within fluorescent images. Values for lung, liver, and whole animal were recorded and averaged with standard error of the mean in Microsoft Excel 2010, and plotted with Graphpad Prizm 5. ImageJ was subsequently used to prepare all montages, with final labeling of figures executed with Microsoft PowerPoint 2010.

2.5. SPECT and CT Imaging and Analysis

SPECT and CT images were acquired with a trimodal Albira PET/SPECT/CT imaging system (Carestream Molecular Imaging, Woodbridge, CT, USA). The Albira system includes a sample platform that passes through the PET, SPECT, and CT mode imaging planes. The gantry platform passes through the PET ring to reach the shared SPECT and CT imaging planes. The Albira system is calibrated to allow for automated fusion of SPECT and CT modalities. The

SPECT and CT systems are calibrated to counts/sec/cc and hounsfield units (HU) respectively.

All mice were measured at 2, 4, and 6 weeks post-injection. Mice were anesthetized with 1.5% isoflurane in an induction box, and received a retro-orbital 1 mCi dose of SPECT tracer ^{99m}Tc-MAA (Cardinal Health, South Bend, IN). Mice were subsequently returned to their cages for 45 minutes to allow for peak ^{99m}Tc-MAA pulmonary bio-distribution. Mice were then anesthetized with Isofluorane again and placed inside the scanner. A 10-minute SPECT scan (60 mm FOV, multi-pinhole collimator, 60 projections) was performed which yielded a 1.8 mm resolution under these parameters. This SPECT scan was followed by a CT scan (110 mm FOV, 45 kVp, 200 µA, at 400 projections). Approximate radiation deep dose equivalent for CT was 220 mSv, and shallow dose equivalent was 357.4 mSv. These doses are over 20-fold lower than reported LD50 values [38]. The SPECT/CT scans were reconstructed using the OSEM and FBP algorithms respectively. This protocol produces a CT image with 250 µm^3 voxels that are sufficient for bulk measurements of lung volume. Note that higher resolution scans may be acquired using this Albira technology with final voxel size of 125 µm^3 or 35 µm^3 to enable sub-tissue region analysis.

SPECT and CT images were quantified using PMOD version 3.2 (PMOD technologies, Zurich, Switzerland). Briefly, SPECT images were analyzed using the "Generate Hot contour ROI 3D" VOI button. Data was analyzed from both the entire range of intensity values, as well as from 66% of the maximum intensity in order to isolate changes in regions of higher intensity signals. To perform normal lung density analysis, CT images were first segmented using the PMOD "tools">"external">"segmentation" operation. Segmentation was set to the range -550 to -200 (HU) and the "create a VOI Template/Mask" check box was created to obtain the normal lung density volume. (The lung density of -550 to -200 HU was identified during preliminary analysis of healthy animals). Image overlays with either SPECT probe or segmented lung volume were collected using the image capture tool in PMOD. ImageJ v1.44 was used to subsequently crop the lungs of each overlay image, and generate a montage of CT, CT with lung segmentation overlay (red), and CT with ^{99m}Tc-MAA SPECT image overlay ("Rainbow" intensity scale).

3. RESULTS

3.1. Assessment of *In Vitro* and *In Vivo* Fluorescent Optical Imaging of DiR Labeled MDA-MB-231 Cells

Preliminary *in vitro* studies were performed to determine the limits and linearity of DiR labeled MDA-MB-231 cell detection. First, DiR MDA-MB-231 cells were serially diluted in two-fold increments in a 96-well plate and imaged (Fig. **1**). Following fluorescent imaging, integrated intensities were recorded for the DiR signal and plotted versus cell count along the left Y-axis of Fig. (**1**). The Target/Background (T/BKG) ratios were also calculated and are given as the right Y-axis. The cell dilution data were subjected to a linear fit with R^2 = 0.99, indicating that integrated intensity comparisons are indicative of labeled cell densities. These results indicated that the *in vitro* cell detection limit for DiR labeled cells approached 1 X 10^3 cells before the T/BKG ratio approached a value of 1.

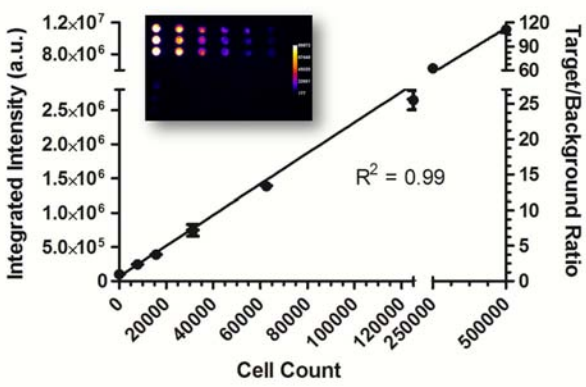

Fig. (1). Limits and linearity of DiR labeled MDA-MB-231 cell *in vitro* fluorescent optical imaging. Serial dilutions of DiR labeled MDA-MB-231 cells in a 96-well plate. Integrated intensity values (left Y-axis) and target/background ratios (right Y-axis) for each well of the dilution series were calculated and plotted versus the diluted cell count.

Next, the protocol for *in vivo* fluorescent optical imaging of DiR labeled MDA-MB-231 cell tracking was assessed. Three mice received 2 x 10^5 DiR labeled MDA-MB-231 cells *via* tail vein injection. No observable signal over background was noted during whole animal fluorescence imaging in these mice after injection (data not shown). Subsequently, three mice were given a 10-fold higher injection of 2 x 10^6 DiR labeled MDA-MB-231 cells *via* the tail vein. These animals were then imaged for whole animal fluorescence at 0, 4, 24, and 48 hours post injection (Fig. **2**, left panel). Integrated intensity analysis of DiR fluorescence was performed at regions of interest around the lung, liver, and whole animal. DiR fluorescence was apparent in the lungs and livers of all animals at all time points imaged. As noted in the images, lung signal was apparent through the entire 48 hours of the experiment, with a modest increase of fluorescent signal of approximately 20% between 4 and 24 hours. Significant liver signal emerged after 4 hours and peaked at over 4-fold higher intensity relative to the post injection image. Note that when DiR was injected alone as a control, significant fluorescence was noted from the liver of the animal, but not the lungs. Fluorescence from the whole animal, including the lungs and liver, doubled by 24 hours and subsequently decreased. When the DiR dye alone was injected into animals, fluorescent signal was readily apparent from the liver region of mice for the 48 hour length of the experiment, while nothing was detected from lungs (Supplementary Fig. **S2**). Since the lungs have previously been shown to have significant tumor burden when MDA-MB-231 cells are injected intravenously [39], cancer cell uptake and proliferation

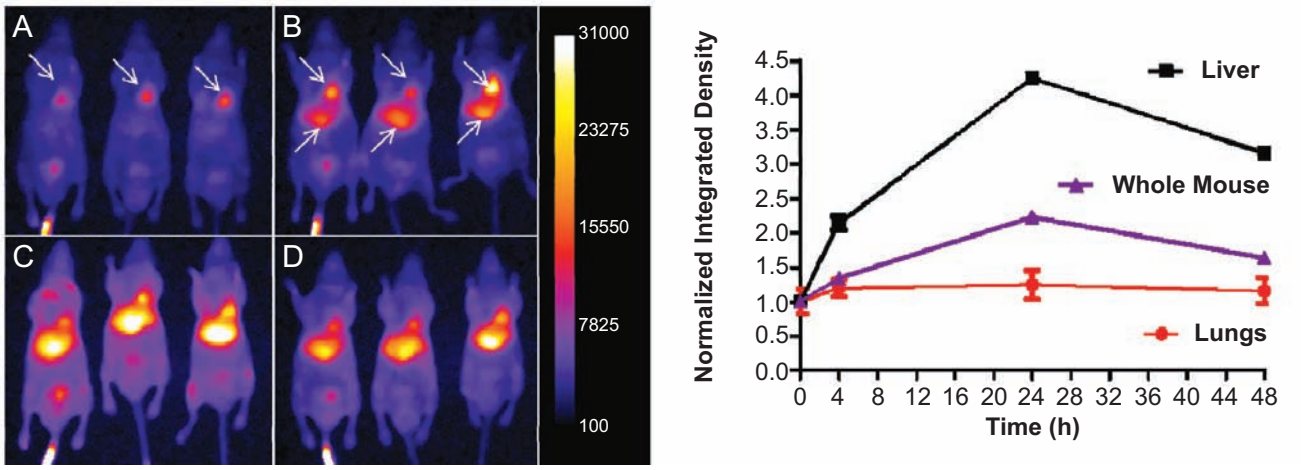

Fig. (2). Preliminary assessment of *in vivo* DiR labeled MBA-MD-231 cell tracking using whole animal fluorescence imaging. Left panel: Three mice were IV injected with 2 x 10^6 DiR labeled MDA-MB-231 cells and subjected to whole animal fluorescence imaging at (**A**) immediately post injection, (**B**) 4, (**C**) 24, and (**D**) 48 hours. Arrows designate the lung and liver locations. Right panel: ROI analysis was performed on the lungs, liver, and whole animal, and normalized values plotted versus time.

at this site was followed for a subsequent six week study.

3.2. *In Vivo* Fluorescent Optical Imaging of DiR Labeled MDA-MB-231 Cells at Outset of Experimental Metastasis Protocol

A preliminary assessment of DiR labeled MDA-MB-231 cells indicated that *in vivo* fluorescent optical imaging will confirm region specific uptake of cells, and function as a positive indicator for successful tail vein injections. Thus, we utilized this method in a separate study in which twelve mice received 2 x 10^6 DiR labeled MDA-MB-231 cells intravenously, and six control mice were injected with saline. All tumor cell bearing animals were subsequently imaged 2 hours post injection to assess the level of DiR fluorescent optical signal in the lungs. Eleven out of twelve mice receiving the tumor cells were found to have DiR fluorescence in their lungs (Supplementary Fig. **S1**). Only mice with fluorescent DiR lung signal, indicative of a successful tail vein IV injection and organ specific cell accumulation were retained to complete the longitudinal SPECT-CT phase of lung imaging.

3.3. SPECT-CT Imaging of Lung Volume and Perfusion in Normal and Diseased Mice

Animals injected with cancer cells, as well as the saline controls, were imaged using a SPECT/CT instrument at 2, 4, and 6 weeks post MDA-MB-231 cell injection. During preliminary image analysis of lung tissue in healthy animals, normal lung density was found to range from -550 to -200 HU. Visualization of segmented (HU range -550 to -200) CT images from healthy animals showed a clear outline of the animals' total lung volume (Fig. **3**, red overlay images). Normal lung segmented volume measurements were used as a marker to assess disease progression in the experimental metastasis model The raw CT images (greyscale), CT images with lung segmentation overlay (in red), and CT images with SPECT ^{99m}Tc-MAA overlay (in rainbow color scheme) of a representative tumor cell injected animal at 2, 4 and 6 weeks post MDA-MB-231 cell injection are shown in Fig. (**3**). A decrease in normal lung density is apparent in raw and segmented CT images with disease progression. Note that these CT data were acquired with a 250 μm isotropic voxel size, thus limiting the resolution of specific tumors. Rather, the current setup enabled visualization and segmentation across the whole volume, in which changes in tissue density were measured across the entire lung.

Results of segmented lung volume analysis for animals enrolled in the experimental metastasis protocol are given in Supplementary Table **S1**, with averages presented in Fig. (**4**). Three animals from the cohort of eleven did not display any reduction in segmented lung volume, despite having bright DiR signal after injection. For these three, either tumor cell colonization was not successful, or subsequent growth was too slow to detect within the six weeks of observation. No tumors were observed during *ex vivo* staining and visual analysis of these lung specimens. The values plotted in Fig. (**4**) omit these animals. Of the remaining eight mice, six had almost 90% reduction in volume, and another two had intermediate losses of 47% and 73%. On average, a normal lung density volume of a healthy animal was found to be in a range 0.33-0.38 ccm for the course of the study. Tumor cell injected animals had a decrease in total normal lung density volume from 0.30 ccm at week 2 post injection, to 0.19 ccm at week 4, and 0.07 ccm at week 6. These mice were found to have significantly lower normal lung density volumes compared to saline control mice at 4 (P-value = 0.03) and 6 weeks (P-value < 0.0001) post injection. Also, animals were sacrificed following CT imaging at 6 weeks and histological examination of lung tissue was performed. Histological examination

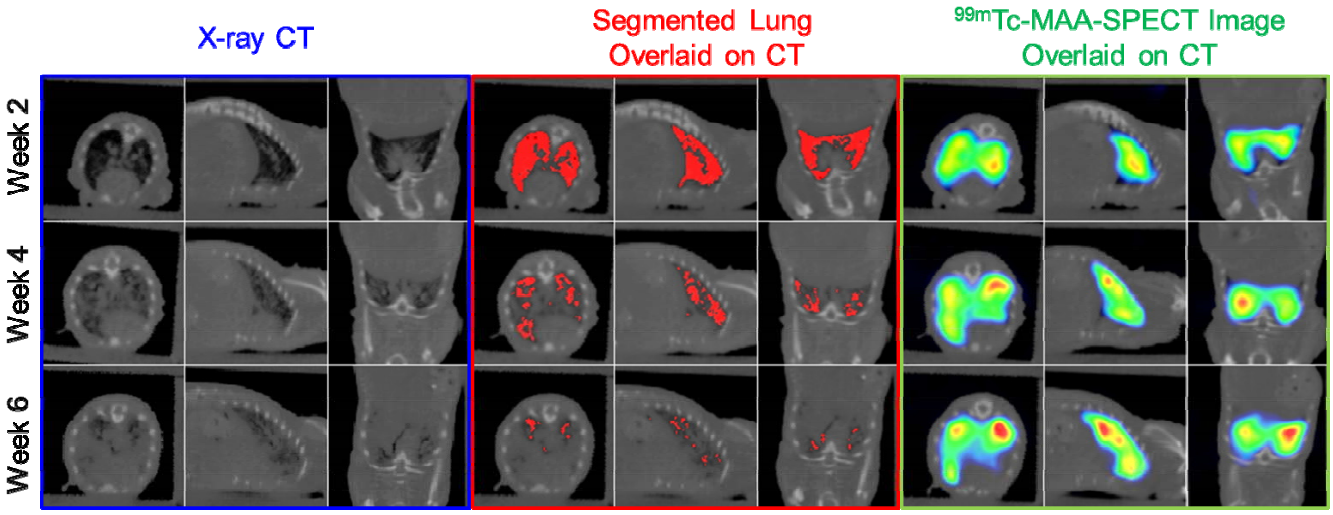

Fig. (3). Representative mouse raw CT, CT with normal lung density segmentation, and SPECT 99mTc-MAA imaging results. Left columns (blue outline): Transverse, sagittal, and coronal X-ray CT slices of the lungs of a tumor bearing mouse, displayed in greyscale at two (top row), four (center row), and six (bottom row) weeks post cancer cell injection. Center columns (red outline): Lung segmentation (HU -550 to -200) shown in red and overlaid on the CT data. Right columns (green outline): SPECT ^{99m}Tc-MAA shown in rainbow intensity scale and overlaid on CT.

revealed a dispersed tumor cell distribution in the lungs of injected mice (Fig. **5**, left frame), which corresponds to the images in the bottom row of Fig. (**3**). Those of the saline animals were clear (Fig. **5**, right frame).

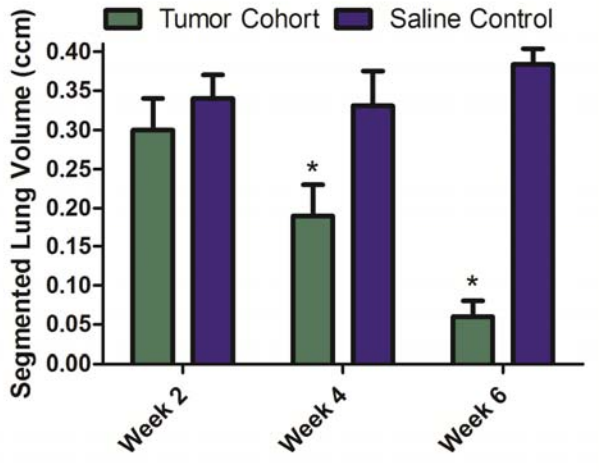

Fig. (4). Normal lung density volume in cancer cell injected and saline control mice at 2, 4 and 6 weeks post injection with MDA-MB-231 cells. (Error bars = standard error of the mean). Statistical significance was noted at week 4 (P-value = .03) and week 6 (P-value < .0001).

In short summation, SPECT imaging with ^{99m}Tc-MAA did not appreciably change with disease progression. Even in the extreme cases in which greater than 95% of lung volume had been overtaken by tumor tissue, the SPECT probe showed perfusion through the entire lung space, without any preferential uptake to given segmented areas (Supplementary Table **S1**). There was no correlation between segmented lung volume from CT and a number of quantitative SPECT outputs, including functional volume, total probe uptake, or thresholded regional uptake intensities.

4. DISCUSSION

Limited reports detailed the use of DiR labeling for whole animal fluorescence imaging of tumor cell tracking. Thus, a preliminary analysis of DiR labeled MDA-MB-231 cells was performed to assess its utility for *in vivo* applications. The cell dilution study noted in Fig. (**1**) demonstrated a linear relationship between fluorescence intensity and cell count. After intravenous injection into live mice, the fluorescent whole body cell tracking was viable for at least 48 hours. Persistent and stable signal was noted from the lung over the entire time course. Interestingly, the liver was identified as another site of cell concentration. However, when the DiR dye alone was injected, it demonstrated a preferential and stable uptake within the liver. Thus, signal at the liver region may be attributed to cell uptake, as well as entrapment of any free dye that might wash out from labeled cells at other sites. This question was not further investigated based on our focus on lung metastasis, as well as prior reports excluding the liver from MDA-MB-231 colonization.

Traditionally, *in vivo* cell tracking has been achieved using cell lines expressing genetic reporters, most commonly luciferase. Bioluminescence imaging provides sensitive luminescence imaging owing to a relatively high signal-to-noise ratio relative to fluorescent imaging. The method for DiR cell tracking applied here and reported elsewhere, provides for sufficient sensitivity owing to the low tissue autofluorescence within these NIR fluorescent imaging parameters. However, this approach is best applied to applications that require cell tracking during a limited time course such that photobleaching, probe wash out, and cell division mediated signal dilution are minimized.

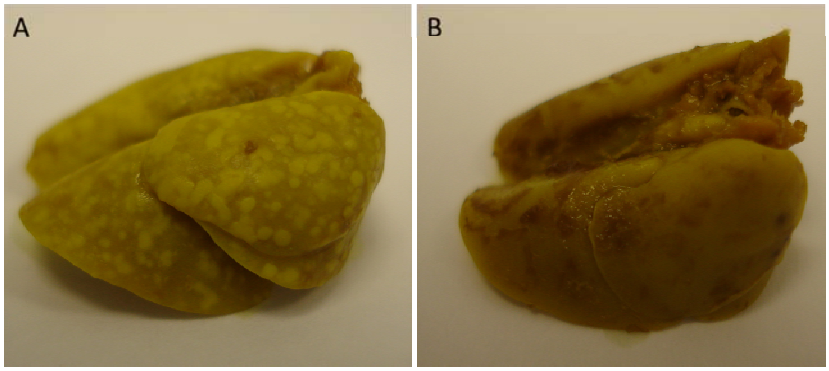

Fig. (5). *Ex vivo* imaging of tumor cell (**A**) and saline (**B**) injected animal lungs from the week six time point, after fixation and staining with Bouin's solution.

Aside from *in vivo* imaging of cell distribution following systemic administration, the exogenous DiR labeling technique described here may also be useful in spontaneous metastasis protocols that use intracardial, femoral artery, intraperitoneal, or even fat pad routes of injection.

A multi-week longitudinal study of tumor cell uptake and proliferation within the lung was subsequently undertaken. As a first step, MDA-MB-231 cells were labeled with DiR and injected into twelve mice. Whole animal fluorescence imaging was subsequently employed to confirm the fidelity of each tail vein injection, and that tissue specific localization within the lungs proceeded as expected. Fluorescent optical signal was detected in the lungs of animals receiving a successful injection, while a single mouse that received a suboptimal injection had no signal from any site. Thus, only one of the twelve animals was excluded from further analysis based on the fluorescent imaging criteria for lung signal.

CT imaging and a computational lung segmentation measurement were employed to monitor disease progression at 2, 4, and 6 weeks of the experimental metastasis protocol. The general assumption of this approach is that the segmented lung volume measurements would have a negative correlation with lung tumor burden. Thus, a decrease in normal lung density is due to an overgrowth of normal lung volume with tumor tissue. As noted in Fig. (**3**), the dark contrast noted from healthy lung diminished over the course of the six weeks for diseased mice indicating a potentially diffuse tumor distribution with disease progression. In fact, *ex vivo* imaging of lungs (Fig. **5**) from tumor mice reveals a diffuse tumor distribution that correlates well with the observed CT lung volume data. Of note, three of eleven animals did not have detectable tumor degradation of lung, while another two had partial degradation. The remaining six had greater than 90% reduction. This distribution of *in vivo* tumor growth is indicative of the challenge of cancer imaging with respect to the heterogeneity that can emerge in an experimentally controlled system. The exact reason for this heterogeneity is unknown, however a failed injection may be excluded due to the presence of fluorescent signal from the lungs after injection. In this case, genetically uniform mouse cohorts were injected with a single cell population derived from cell culture of a commonly used and thoroughly characterized cell line. DiR labeling and optical imaging showed that each of the eleven animals received a proper injection, and cells localized to the lung tissue. Nevertheless, in terms of average values for the eight animals with measureable decline, the volume at week two was not statistically different from control, while a marked decrease to values of 0.19 and 0.07 was noted at weeks 4 and 6 respectively.

These results indicate that longitudinal CT imaging provides a solid platform with which to perform analysis of metastatic cancer growth in the lung. This technique can readily be applied to genetically altered cell types such that molecular or biochemical pathways may be coupled with the disease progression information provided with CT. For example, using this technique it could be possible to evaluate changes in metastatic properties of tumor cell lines with altered expression of a gene product with a suspected, but unconfirmed role in lung metastasis. The initial administration of the mutant cell line would be confirmed using DiR cell tracking, while metastatic lung tumor progression would be monitored through subsequent CT imaging. Changes in metastatic tumor progression at specific phases of metastasis with mutant versus WT cell lines may implicate and partially reveal the role of a given gene in metastasis.

At each time point, a SPECT scan with ^{99m}Tc-MAA was performed in concert with the CT, such that the animal was not moved and lung perfusion data would be directly compared to segmented lung values. We hypothesized that tumor associated reduction in lung volume would alter the perfusion profile of the MAA nuclear probe. These scans yield a resolution of 1.8 mm which would be sufficient to measure changes within murine lung volumes that typically exceed 0.3 ccm (300 mm^3). During these studies, ^{99m}Tc-MAA SPECT imaging did not reveal any change in lung vascular function with disease progression. Three SPECT parameters including functional volume, total uptake, and threshold lung region specific uptake were measured and compared to the lung segmentation data. No correlation was found after vigorous analysis

(data not shown). Histological examination of lung tissues revealed a dispersed profile of smaller tumors present throughout the tissue, rather than larger tumors that might be associated with altered or damaged vasculature (Fig. **5**). Given these histological findings, it is not surprising that perfusion imaging did not reveal any significant change in lung vasculature function. Even in the case of moderate tumor growth, it is possible that damage to native host tissue could be offset by angiogenesis promoted by tumors, and that ^{99m}Tc-MAA SPECT imaging would not detect any net changes in vascular function. Nevertheless, ^{99m}Tc-MAA SPECT imaging may prove useful when mediators of angiogenesis in tumor growth are specifically evaluated, or when imaging the necrotic core of a larger tumor within the lung space.

5. CONCLUSION

Metastatic breast cancer (stage IV) has a significantly decreased survival rate relative to other forms of breast cancer. Currently, metastatic breast cancer patients are treated with a combination of chemotherapeutics and targeted therapies; however, not all patients respond to these treatments and many will also develop resistance to the chemotherapeutics. It is important and necessary to further understand the important molecular mechanisms involved in metastasis in order to develop targeted therapies to treat this deadly disease. Using classical methods, scientists have studied experimental metastasis in mice by injecting engineered tumor cell lines intravenously *via* the tail vein followed by necropsy and histological methods. Here, we have demonstrated the use of non-invasive imaging strategies to enhance the information content gleaned form *in vivo* models of metastasis. We show that utilizing DiR staining of cells is sufficient to determine efficiency of intravenous injections as well as track cells to their site of metastasis. Further, we show that small tumor models can be effectively monitored for disease progression by using X-ray CT imaging. These findings provide improvements to the classical *in vivo* experimental metastases assay that will be useful in understanding molecular mechanisms implicated in the metastasis of breast and other types of cancers.

ABBREVIATIONS

^{99m}Tc-MAA = Technetium ^{99m}Tc macro aggregated albumin

A.U. = Arbitrary Units

CCM = Cubic Centimeters

CT = Computed Tomography

DiR = 1,1′-Dioctadecyl-3,3,3′,3′-Tetramethylindotricarbocyanine Iodide

FBP = Filtered Back Projection

HU = Hounsfield Units

IV = Intravascular

kBq = Kilobecquerel

MRI = Magnetic Resonance Imaging

NIR = Near-Infrared

OSEM = Order Subset Expectation Maximization

PET = Positron Emission Tomography

SPECT = Single Photon Emission Computed Tomography

CONFLICT OF INTEREST

Todd A. Sasser is an employee of Carestream Molecular Imaging. W. Matthew Leevy is a former full time employee for Carestream Molecular Imaging, and currently works for them in a consulting role.

ACKNOWLEDGEMENTS

Z.T.S. is the recipient of a V Scholar Award from the V Foundation for Cancer Research. W.M.L. warmly thanks Carestream Health Molecular Imaging for contributing funds to purchase radioisotopic SPECT probes for this study. The authors thank Jenna Leevy for significant editing assistance.

SUPPLEMENTARY MATERIAL

Supplementary material is available on the Publisher's web site along with the published article.

REFERENCES

[1] Hanahan D, Weinberg RA. Hallmarks of cancer: the next generation. Cell 2011; 144(5): 646-674.

[2] Paweletz, CP, Charboneau L, Liotta LA. Overview of metastasis assays In: Current Protocols in Cell Biology. John Wiley & Sons, Inc. 2001; 19.1.1-19.1.9.

[3] Glondu M, Liaudet-Coopman E, Derocq, Platet N, Rochefort H, Garcia M. Down-regulation of cathepsin-D expression by antisense gene transfer inhibits tumor growth and experimental lung metastasis of human breast cancer cells. Oncogene 2002; 21(33): 5127-5134.

[4] Minn AJ, Gupta GP, Siegel PM, *et al*. Genes that mediate breast cancer metastasis to lung, Nature 2005; 436(7050): 518-524.

[5] Grossoni VC, Todaro LB, Kazanietz MG, de Kier Joffe ED, Urtreger AJ. Opposite effects of protein kinase C beta1 (PKCbeta1) and PKCepsilon in the metastatic potential of a breast cancer murine model. Breast Cancer Res Treat 2009: 118(3): 469-480.

[6] Elkin M, Vlodavsky I. Tail vein assay of cancer metastasis In: Current Protocols in Cell Biology. John Wiley & Sons, Inc. 2001; 19.2.1-19.2.7.

[7] Vines DC, Green DE, Kudo G, Keller H. Evaluation of mouse tail-vein injections both qualitatively and quantitatively on small-animal PET tail scans. J Nucl Med Technology 2011; 39(4): 264-270.

[8] Kiessling F. Non invasive cell tracking In: Handbook of Experimental Pharmacology. Berlin Heidelberg Springer-Verlag 2008; 305-321.

[9] de Almeida PE, van Rappard JR, Wu JC. *In vivo* bioluminescence for tracking cell fate and function. Am J Physiol Heart Circ Physiol 2011; 301: H663-H671.

[10] Pesnel S, Pillon A, Créancier L, *et al*. Optical imaging of disseminated leukemia models in mice with near-infrared probe conjugated to a monoclonal antibody. PLoS One 2012; 7(1): e30690.

[11] Keyaerts M, Remory I, Caveliers V, *et al.* Inhibition of firefly luciferase by general anesthetics: Effect on *in vitro* and *in*

vivo bioluminescence imaging. PLoS One 2012; 7(1): e30061.
[12] Kalchenko V, Shivtiel S, Malina V, *et al*. Use of lipophilic near-infrared dye in whole-body optical imaging of hematopoietic cell homing. J Biomed Opt 2006; 11(5): 050507-050507.
[13] Eisenblätter M, Ehrchen J, Varga G, *et al*. *In vivo* optical imaging of cellular inflammatory response in granuloma formation using fluorescence-labeled macrophages. J Nucl Med 2009; 50(10): 1676-1682.
[14] Li Y, Yao Y, Sheng Z, Yang Y, Ma G. Dual-modal tracking of transplanted mesenchymal stem cells after myocardial infarction. Int J Nanomedicine 2011; 6: 815-823.
[15] Sutton EJ, Boddington SE, Nedopil AJ, *et al*. An optical imaging method to monitor stem cell migration in a model of immune mediated arthritis. Opt Express 2009; 17(26): 24403-24413.
[16] Lassailly F, Griessinger E, Bonnet D. "Microenvironmental contaminations" induced by fluorescent lipophilic dyes used for noninvasive *in vitro* and *in vivo* cell tracking. Blood 2010; 115(26): 5347-5354.
[17] Johnson KA. Imaging techniques for small animal imaging models of pulmonary disease: micro-CT. Toxicol Pathol 2007; 35(1): 59-64.
[18] Froese AR, Ask K, Labiris R, *et al*. Three-dimensional computed tomography imaging in an animal model of emphysema. Eur Respir J 2007; 30(6): 1082-1089.
[19] Artaechevarria X, Pérez-Martin D, Ceresa M, *et al*. Airway segmentation and analysis for study of mouse models of lung disease using micro-CT. Phys Med Biol 2009; 54(22): 7009-7024.
[20] Lederlin M, Ozier A, Montaudon M, et al. Airway remodeling in a mouse asthma model assessed by in-vivo respiratory-gated micro-computed tomography. Eur Radiol 2010; 21(1): 128-137.
[21] Kennel JK, Davis IA, Branning J, Pan H, Kabalka GW, Paulus MJ. High resolution computed tomography and MRI for monitoring lung tumor growth in mice undergoing raioimmunotherapy: Correlation with histology. Med Phys 2000; 27(5): 1101-1107.
[22] Cavanaugh D, Johnson E, Price RE, Kurie J, Travis EL, Cody DD. *In vivo* respiratory-gated micro-CT imaging in small-animal oncology models. Molecular Imaging 2004; 3(1): 55-62.
[23] Winkelmann CT, Figueroa SD, Rold TL, Volkert WA, Hoffman TJ. Microimaging characterization of a B16-F10 melanoma metastasis mouse model. Molecular Imaging 2006; 5(2): 105-114.
[24] Li XF, Zanzonico P, Ling CC, O'Donoghue J. Visualization of experimental lung and bone metastasis in live nude mice by X-ray micro-computed tomography. Technol Cancer Research Treat 2006; 5(2): 147-155.
[25] Greschus S, Savai R, Wolf JC, *et al*. Non-invasive screening of lung nodules in mice comparing a novel volumetric computed tomography with a clinical multislice CT. Oncol Rep 2007; 17: 707-712.
[26] Hori Y, Takasuka N, Mutoh M, *et al*. Periodic analysis of urethane-induced pulmonary tumors in living A/J mice by respiration-gated X-ray microcomputed tomography. Cancer Sci 2008; 99(9): 1774-1777.
[27] Haines BB, Bettano A, Chenard M, *et al*. Micro-CT imaging of lung tumors in mice. Neoplasia 2009; 11: 39-47.
[28] Fushiki H, Kanoh-Azuma T, Kotah M, *et al*. Quantification of mouse pulmonary cancer models by microcomputed tomography imaging. Cancer Sci 2009; 100(8): 1544-1549.
[29] Namati E, Thiesse J, Sieren JC, Ross A, Hoffman EA, McLennan G. Longitudinal assessment of lung cancer progression in the mouse using *in vivo* micro-CT imaging. Med Phys 2010; 37(9): 4793-4804.
[30] Martiniova L, Kotys MS, Thomasson D, *et al*. Non-invasive monitoring of a murine model of metastatic pheochromocytoma: a comparison of contrast enhanced and non-enhanced MRI. J Magn Reson Imaging 2009; 29(3): 685-691.
[31] Kirsch DG, Grimm J, Guimaraes AR, *et al*. Imaging primary lung cancers in mice to study radiation biology. Int J Radiat Oncol Biol Phys 2010; 76(4): 973-977.
[32] Zöphel K, Bacher-Stier C, Pinkert J, Kropp J. Ventilation/perfusion lung scintigraphy: what is still needed? A review considering technetium-99m-labeled macro-aggregates of albumin. Ann Nucl Med 2009; 23: 1-16.
[33] Wietholt C, Roerig DL, Gordon JB, Haworth ST, Molthen RC, Clough AV. Bronchial circulation angiogenesis in the rat quantified with SPECT and micro-CT. Eur J Nucl Med Mol Imaging 2008; 35: 1124-1132.
[34] Joimel U, Gest C, Soria J, *et al*. Stimulation of angiogenesis resulting from cooperation between macarophages and MDA-MB-231 breast cancer cells: proposed molecular mechanism and effect of tetrathiomolybate. BMC Cancer 2010; 10: 375.
[35] Correa de Sampaio P, Auslaender D, Krubasik D, *et al*. A heterogeneous *in vitro* three dimensional model of tumour-stroma interactions regulating sprouting angiogenesis. PloS One 2012; 7(2): e30753.
[36] Hamami ME, Poeppel TD, Müller S, *et at*. SPECT/CT with 99mTc-MAA in radioembolization with 90Y microspheres in patients with hepatoceullular cancer. J Nucl Med 2009; 50(5): 888-892.
[37] Cailleau R, Olive M, Cruciger QV. Long-term human breast carcinoma cell line of metastatic origin: preliminary characterization. *In Vitro* 1978; 14: 911-915.
[38] Patchen ML, MacVittie TJ, Souza LM. Postirradiation treatment with granulocyte colony-stimulating factor and preirradiation WR-2721 administration synergize to enhance hemopoietic reconstitution and increase survival. Int J Radiat Oncol Biol Phys 1992; 22(4): 773-779.
[39] Lee WJ, Chen WK, Wang CJ, Lin WL, Tseng TH. Apigenin inhibits HGF-promoted invasive growth and metastasis involving blocking PI3K/Akt pathway and beta 4 integrin function in MDA-MB-231 breast cancer cells. Toxicol Appl Pharmacol 2008; 226(2): 178-191.

Received: August 06, 2012 Revised: October 12, 2012 Accepted: October 15, 2012